Electrochemical Performance and Microstructure Characterization of Nickel Yttrium-Stabilized Zirconia Anode

Jingbo Liu
Texas A&M University-Kingsville, Dept. of Chemistry, 700 University Blvd., Kingsville, TX 78363

Viola Birss
University of Calgary, Dept. of Chemistry, 2400 University Dr., Calgary, AB, T2N 1N4, Canada

Josephine Hill
University of Calgary, Dept. of Chemical Engineering, 2400 University Dr., Calgary, AB, T2N 1N4, Canada

DOI 10.1002/aic.12080
Published online October 29, 2009 in Wiley InterScience (www.interscience.wiley.com).

A nickel and yttrium-stabilized zirconia (Ni-YSZ) composite is one of the most commonly used anode materials in solid oxide fuel cells (SOFCs). One of the drawbacks of the Ni-YSZ anode is its susceptibility to deactivation due to the formation of carbonaceous species when hydrocarbons are used as fuel supplies. We therefore initiated an electrochemical study of the influence of methane (CH_4) on the performance of Ni-YSZ anodes by examining the kinetics of the oxidation of CH_4 and H_2 over operating temperatures of 600–800°C. Anode performance deterioration was then correlated with the degree of carbonization observed on the anode using ex-situ X-ray powder diffraction and scanning electron microscopy techniques. Results showed that carbonaceous species led to a significant deactivation of Ni-YSZ anode toward methane oxidation. © 2009 American Institute of Chemical Engineers *AIChE J,* 56: 1651–1658, 2010
Keywords: composite, solid oxide fuel cell, coke formation, characterization, electrochemical performance

Introduction

Fuel cells are green energy resources that can spontaneously convert chemical energy into electrical energy, releasing heat, and water during the electrochemical reaction.[1–3] One class of fuel cells is drawing significant attention: solid oxide fuel cells (SOFCs), which can be thought of as having a ceramic membrane composed of yttrium-stabilized zirconia (YSZ), as the electrolyte; hydrogen or hydrocarbon (for example CH_4) as fuel supplies; and metal or metal ceramic composite as the catalysts.[4–7] SOFCs (Figure 1) provide direct current for stationary and portable applications, such as to power automotives, lights, or other electrical appliances.

The advantages of SOFCs are ultrahigh energy conversion efficiency, ultralow emission of environmental pollutants, simplicity in design and operation, and flexibility of fuel supplies. However, the current SOFCs designs encounters problematic issues, manufacturing expense, performance degradation over prolonged use, heat retention, limited operating temperature ranges, and materials compatibility.[8–10] In an SOFC, the state-of-the-art electrolyte is yttrium-stabilized zirconia (YSZ), a polycrystalline ceramic that allows oxide ions (O^{2-}) to conduct through the electrolyte from the cathode to the anode compartment.[11,12] The most-frequently used anode materials in SOFC are porous metal and ceramic composite composed of Ni and nickel and yttrium-stabilized

Correspondence concerning this article should be addressed to J. Liu at this current address: MSC 161, 700 University Blvd., Kingsville, TX; e-mail: kfjll00@tamuk.edu.

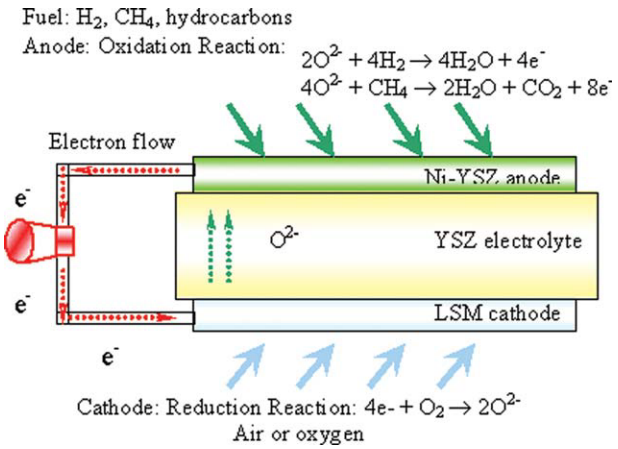

Figure 1. Simplified schematic design of SOFCs.

[Color figure can be viewed in the online issue, which is available at www.interscience.wiley.com.]

zirconia (Ni-YSZ), which have excellent catalytic properties and conduct current efficiently, but are found to deteriorate over prolonged time and become deactivated because of carbonaceous species formation (also defined as coke formation when hydrocarbon are used as fuel supplies) at the anode.[13,14] Therefore, it is critical to clarify the mechanism of coke formation on the surface of Ni-YSZ anodes by monitoring the electrochemical properties and by characterizing the microstructure of the anodes with prolonged exposure to CH_4.[15–17] CH_4 as the SOFCs fuel supply recently received increasing attention as CH_4 is electrochemically oxidized to produce synthesis gas (syngas) and electricity with ultralow environmental pollution.[18–20] As mentioned earlier, coke formation causes rapid degradation of anode performance. The carbonaceous deposition takes place through catalytic dissociative adsorption of CH_4 on the anode electrode surface, which becomes problematic[21–23] Coke formation is one of the main causes of anode catalyst deactivation in catalytic reactions involving hydrocarbon transformation.[24,25] It is well-established that surface carbonaceous species leading to coke formation can also become major reaction intermediates in several catalytic process like C_8 and Ni_3C formation.[26,27] To improve the performance of catalytic materials, it is important to obtain in-depth insight into the surface chemistry of CH_4 dissociative adsorption and the nature of the various carbonaceous species formed on the anode surface.[28,29]

In this study, the overall aim was to clarify the mechanism of coke formation on the surface of Ni-YSZ anodes by measuring the electrochemical properties and characterizing the microstructure as complementary techniques when the anode is exposed to a CH_4 fuel supply. An electrochemical method for monitoring coke accumulated on the surface of Ni-YSZ anode is to measure the charge-transfer resistance (R_{ct}) and exchange-current density (i_o) before and after exposure to CH_4. *Ex-situ* X-ray powder diffraction (XRD) and scanning electron microscopy (SEM) were employed to determine the structural, morphological, and elemental changes of the Ni-YSZ anode. The novelties of this research are: (1) combining electrochemical technique and state-of-the-art instrumentation to understand coke formation mechanism; and (2) using cost-effective green chemistry to derive the nanostructured composites to act as anode materials. The contributions of this article are: (1) providing fundamental study on coke formation; combining (2) offering guidance for SOFC performance improvement; and (3) optimizing the green fabrication variables for the SOFC anode materials.

Experimental

All chemicals, unless otherwise specified, were obtained from Sigma-Aldrich (St. Louis, MO), and solvents were obtained from VWR International (West Chester, PA). The reagents were reagent grade and were used without further purification. Doubly distilled and 0.2 micron-filtered (Milli-Q) water was used in the dissolution of our compounds.

Anode construction

The anode materials were fabricated using cost-effective Sol-Gel (SG) method followed by heat-treatment (Figure 2). The starting materials 0.044 mol nickel chloride ($NiCl_2$) and 0.00488 mol yttrium nitrate $Y(NO_3)_3$ were dissolved in 50 ml 50% aqueous ethanol (v/v). The alkoxide 0.056 mol zirconium butoxide $Zr(OBu)_4$ was dispersed in 20 ml 1-butanol and then incrementally added into the above solution. The reducing agent ascorbic acid was added in excess, and dissolved in water to form an aqueous solution which was incrementally added into the above solution to reduce Ni^{2+} cation to metallic Ni. The sol-precursor was obtained on agitation under 1000 revolutions per minute (rpm) and refluxing for 2 h, and its viscosity was adjusted at 10.5 centistokes via evaporating ethanol carefully. This Ni-YSZ sol-precursor was screen-printed onto the YSZ electrolyte substrate. After deposition of each layer, the anode wafer was preheated at 110°C for 30 min to remove the solvent. In total, five layers were deposited on the YSZ substrate. The layered Ni-YSZ/YSZ wafers heated at temperatures ranging from 600 to 900°C with heating rate of 5°C/min. The increment in temperature was controlled at 50°C and each temperature was maintained for 4 h to obtain highly crystalline composite and to increase adhesion between the anode and electrolyte support. It was found that heating temperature at 900°C was

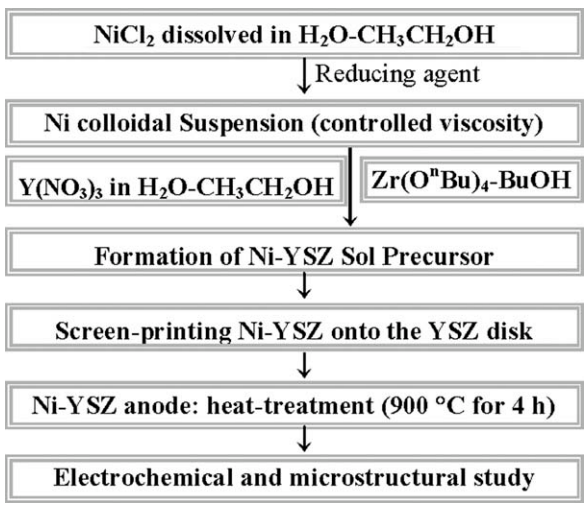

Figure 2. The flowchart of anode materials fabrication.

the optimal. The Ni-YSZ/YSZ anode was then placed in the electrochemical half-cell configuration by heating the assembly from 25 to 800°C under reducing atmosphere (H_2 or CH_4). The surface area of anode was kept between 0.2 to 0.3 cm^2, which was used as the working electrode (WE). The reference electrode (RE) with a small surface area (approximately 0.05 cm^2) was deposited on the same side as WE. On the opposite side, the Ni-YSZ was used as the counter electrode (CE) with an area larger than that of the WE to remove the electrons promptly.

The YSZ substrate was fabricated using commercially available YSZ powder. The YSZ powder was pressed into a disc with diameter 1.5 cm. This disk was heated at 1350°C for 4 h to obtain the half fuel cell with sufficient mechanical strength. The current collectors, made of platinum (Pt) gauze, were then attached to the RE, CE, and WE using conductive Pt paste.

Electrochemical analysis

Half-cell experiments were carried out at temperatures ranging from 600 to 800°C (in increments of 50°C) in a tube furnace using water-saturated H_2 or CH_4 as the fuels. The H_2 flow rate was set at 20 ml/min and CH_4 flow rate at 2.2 ml/min. The low flow rate for CH_4 was used to obtain highly distributed carbonaceous deposition. For the electrochemical impedance (EIS) analyses, a Solartron 1255 frequency response analyzer coupled with the potentiostat was used. The frequency varied from 100,000 Hz to 0.05 Hz, and the measurements were carried out using a 10 mV perturbation amplitude at the open circuit potential (OCP). The impedance measurements and fitting analyses were carried out with commercial software (ZPLOT). Cyclic voltammetry (CV) experiments were performed using an Solartron 1287 interface. The sweep rates range from 2 to 400 mV/s with data collection handled by Corrware software™. The current-resistance (IR) drop originating from the electrolyte resistance was compensated using positive feedback or current interruption techniques to establish the resistance-free exchange current and applied potential (i/η) characteristics.[30]

All of the electrochemical experiments were carried out in the fuel cell set-up shown in Figures 3a, b. To reduce the electrical noise during the experiments, a nichrome coil (not shown in the figure) was placed around the quartz tube. In this three-electrode CV and impedance experiments, Pt gauze, attached to a Pt wire, was press-contacted to the Ni-YSZ and Pt paste electrodes with the aid of a spring loaded ceramic cap, thus serving as current collectors. A coke formation study was conducted with CH_4 flowing into the SOFC compartment at open circuit for various periods of time (0.5 to 4 h) at temperatures ranging from 600 to 800°C in increment of 50°C. The carbonaceous deposits were removed by heating the SOFC in air to reuse the Ni-YSZ anode.[31,32]

Microstructural analysis

X-ray Diffraction (XRD) technique was employed to determine the crystalline phase and average crystallite size of the Ni-YSZ anode. The XRD patterns were collected using a Rigaku multiflex diffractometer (Department of Geology and Geophysics, University of Calgary), equipped with a copper (Cu) source. Operating voltage and current were controlled at 40 kV and 40 mA, respectively. The scanning range was varied between 20° and 80° at a rate of 2 degree/min and high-resolution XRD was employed at scanning rate of 0.05 degree/min. The average crystallite size and lattice constant variables were calculated using the Jade 7.0 software. The surface morphology, the cross-sectional images, and the thickness of the Ni-YSZ anode layer were determined using a Philips environmental scanning electron microscope (FEI ESEM) equipped with X-ray energy dispersive spectroscope (EDS, Health Sciences Center, University of Calgary). An accelerating voltage of 20 kV and high vacuum of ca. 1.0×10^{-5} mbar were generally employed. The Ni-YSZ anode wafers were mechanically fractured using a diamond blade, enabling an easier estimation of the film thickness. The samples were attached to aluminum (Al) stubs using conducting carbon tape (E. T. Enterprises) and then sputter-coated with a thin layer of gold (Au)/palladium (Pd) to improve the surface conductivity. A Tecnai F20 G^2 transmission electron microscope (TEM) (Imaging and Microscope Center, Texas A&M University-College Station)

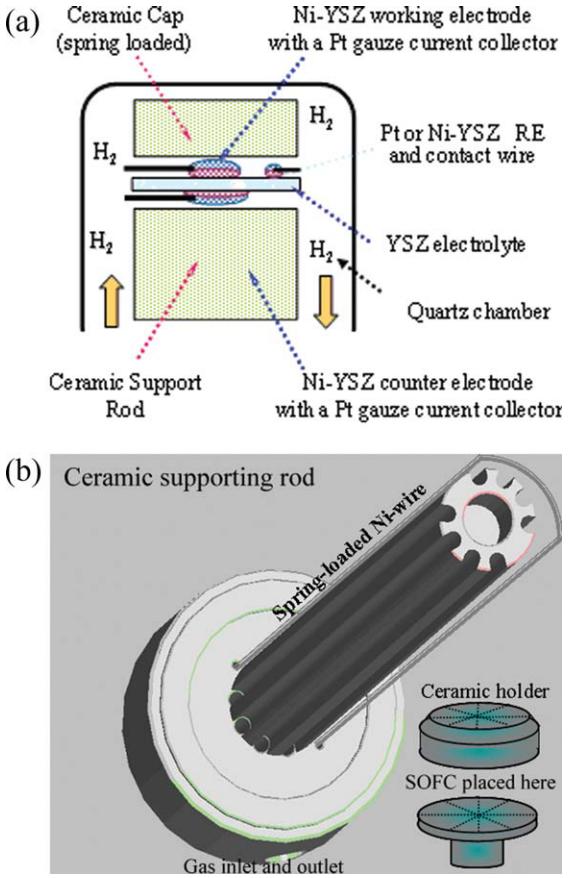

Figure 3. (a) The Experimental set-up of electrochemical analysis via three-electrode technique: high temperature design; (b) the Experimental set-up of electrochemical analysis: sample holder and supporting rod.

[Color figure can be viewed in the online issue, which is available at www.interscience.wiley.com.]

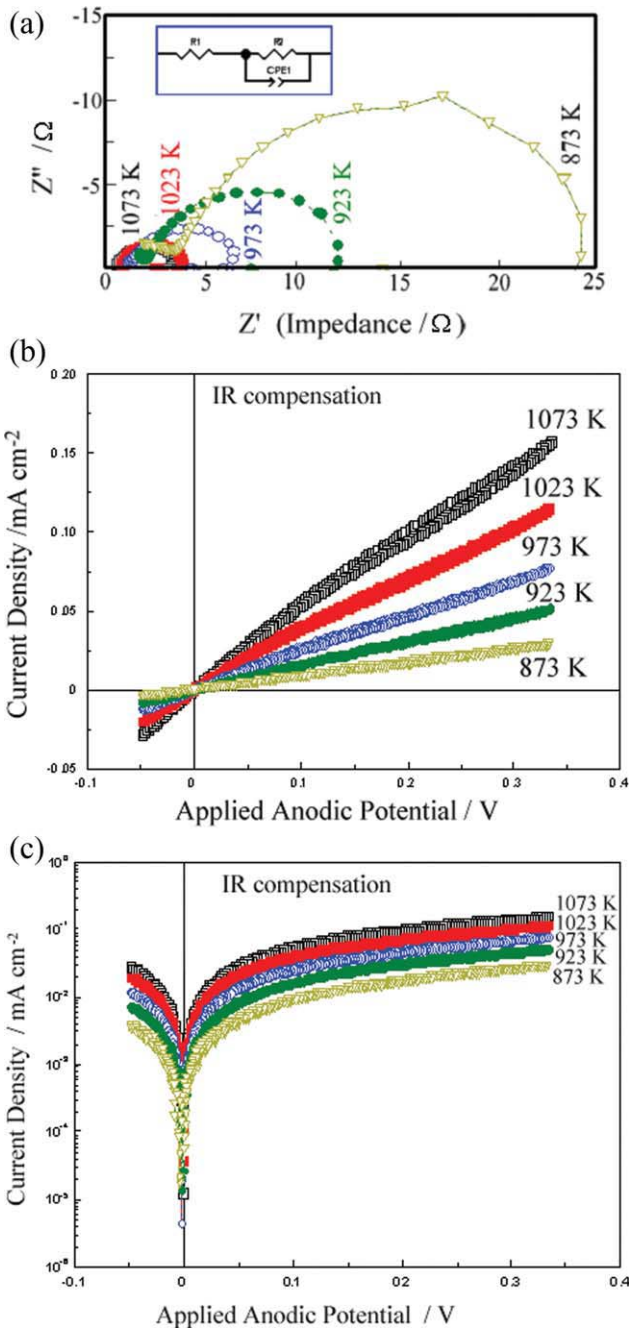

Figure 4. (a) EIS data of HOR on a Ni-YSZ anode (0.11 cm^2) taken at temperatures indicated (3 vol % H_2O saturated H_2 at flow rate of 20 mL/min. Data taken from 105 to 0.05 Hz). (b) Low-field CV data of HOR on a Ni-YSZ anode (0.11 cm^2) taken at temperatures indicated (3 vol % H_2O saturated H_2 at flow rate of 20 mL/min, applied anodic potential of 0.0 to 0.7 V). (c) High-field CV data of HOR on a Ni-YSZ anode (0.11 cm^2) taken at temperatures indicated (3 vol % H_2O saturated H_2 at flow rate of 20 mL/min. Data taken from 0.0 to 0.7 V).

[Color figure can be viewed in the online issue, which is available at www.interscience.wiley.com.]

equipped with postcolumn Gatan Image Filter was used to characterize the nanostructured SOFC particles. Magnifications were calibrated using standards of commercial cross-line grating replica and SiC lattice images.[33,34]

Results and Discussion

Determination of H_2 oxidation kinetics

The kinetics of H_2 oxidation reaction is defined by the exchange current density (i_o), which can be measured using three-electrode techniques. One of the approaches, electrochemical impedance spectroscopy (EIS) commonly known as alternating current (AC) impedance was carried out on the Ni-YSZ/YSZ anode, as shown in Figure 4a. High frequency noise and inductance were sometimes observed during the measurements, generally attributed to the instrument and the leads. At intermediate and low frequencies, only one reasonably established semicircle was observed for hydrogen oxidation reaction (HOR) on Ni-YSZ/YSZ anodes at all temperatures. Thus, HOR has been modeled using a simple R_s, charge transfer resistance/constant phase element (R_{ct}/CPE) circuit, as shown in the insert of Figure 4a. R_1 (also denoted as R_s) corresponded to the series resistance, arising from the contacts, leads, and the resistance of the electrolyte and/or between the working electrode (WE) and reference electrode (RE). R_2 is also denoted as R_{ct} to represent charge transfer resistance. With increasing temperature, both R_s and R_{ct} (Table 1) are observed to decrease exponentially, which indicated faster kinetics at higher temperature due to the faster ionic conduction.

For a simple system, i_o can be obtained from the diameter (charge transfer resistance, R_{ct}) of the Nyquist plot[35] and calculated using Eq. 1,

$$i_o = \frac{R \times T}{n \times F} R_{ct} \tag{1}$$

where R is the ideal gas constant, 8.314 J/(mol K); T is the operating temperature in Kelvin; n is the total number of electrons transferred for the HOR ($n = 4$); and F is the Faraday constant 96,485 C/mol, respectively.[36] The low-field and high-field cyclic voltammetry (CV) results shown in Figures 4b, c also indicate an exponential dependence of exchange current density on operating temperatures when different overpotential were applied. All CVs' plots shown in this article are corrected for the IR drop using R_s obtained from the EIS measurements. All current densities refer to the geometric WE surface area. At low applied potentials (low field Figure 4b) i_o was also determined by using Eq. 2 of the low-field approximation,[31]

Table 1. The Exchange Current Density of HOR on Ni-YSZ/YSZ Anode at Various Operating Temperatures (Three Techniques Used)

Temperature (K)	R_s (W/cm^2)	R_{ct} (W/cm^2)	i_o (mA/cm^2)		
			EIS	LF	HF
873	4.83	26.31	1.43	3.20	6.37
923	2.49	12.34	3.22	5.99	11.49
973	1.70	6.81	6.16	9.49	16.79
1023	1.07	3.96	11.14	14.78	29.09
1073	0.66	2.38	19.42	21.22	41.10

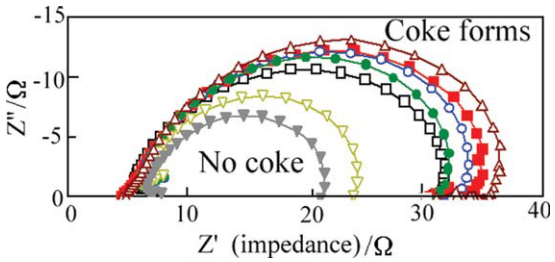

Figure 5. HOR on a Ni-YSZ anode (0.11 cm^2) taken at 700°C, OCP, 10 mVrms, and 105 to 0.05, CH_4: 2.2 mL/min, water saturated, exposure to CH_4 for various time period).

[Color figure can be viewed in the online issue, which is available at www.interscience.wiley.com.]

$$i_o = \frac{R \cdot T \cdot v}{n \cdot F} \text{slope} \tag{2}$$

where v is the number of occurrence of the rate determining step and slope is derived from the plot of current density as a function of anodic potential (η) in the low-field region (generally from −0.1 to 0.2 V).

For the high-field approximation, i_o can be obtained from the y-intercept of the log i/η plot (Figure 4c) and calculated using equation of high-field approximation (3),

$$i_o = 10^{y-\text{intercept}} \tag{3}$$

The value of y-intercept is derived from the intersection of the ordinate and tangent of the logarithms of current density as a function of anodic potential. Values for i_o obtained from the three techniques (AC impedance, low-field, and high-field CV) are tabulated in Table 1. It is observed that the i_o from the low-field method increases from 1.4 mA/cm^2 to 20 mA/cm^2 by increasing the cell temperature from 600 to 800°C. AC impedance i_0 values essentially correspond to the IR-compensated low-field CV data. However, the i_o obtained from the high-field CV results deviate from these values. This may indicate that the polarization potentials are not sufficiently positive, which is mainly limited by the instrument capacity.

Deactivation of anode reactivity due to coke formation

To study coke formation, H_2O-saturated CH_4, with flow rate of 2.2 ml/min, was supplied to the SG-derived Ni-YSZ anode compartment. The activity of a Ni-YSZ anode decreased dramatically with the introduction of CH_4. Figure 5 displays the AC impedance data collected at the OCP and operating temperature is controlled at 700°C. It can be readily seen that the diameter of the impedance is increased from 6.8 Ω/cm^2 to 12.1 Ω/cm^2 (30 min exposure to CH_4) and then further down 20 (45 min), 25 Ω/cm^2 (60 min), indicating that carbonaceous species were deposited onto the surface of anode, which diminished the activity of the Ni catalyst. Polarization resistance increases with prolonged exposure to CH_4 and eventually, the Ni-YSZ anode deteriorates completely. It is reasonable to assume that the carbonaceous deposition accompanies pore closure and/or encapsulation

Table 2. The Charge Transfer Resistance (R_p) and Exchange Current Density (i_o) Upon Exposure of Ni-YSZ/YSZ Anode to CH_4 (Data Collected at 700°C, OCP, 10 mVrms, and 10^5 to 0.05 Hz, Exposure to CH_4 for Various Time Period)

Exposure Time (min)	R_{ct} (W/cm^2)	Exchange Current Density (mA/cm^2)
0	6.81	6.16
30	12.10	3.49
45	20.02	2.10
60	25.42	1.66
120	28.24	1.48
180	30.52	1.36

of the electrochemically active sites, causing the anode activity to decrease continuously with the cycling time.[10] Correspondingly, the exchange current density decreased from 6.16 to 1.36 and eventually to 0 mA/cm^2 as shown in Table 2.

Structural studies by X-ray powder diffraction

XRD was employed to identify the crystalline phase of the Ni, YSZ, and carbonaceous species caused by the coke

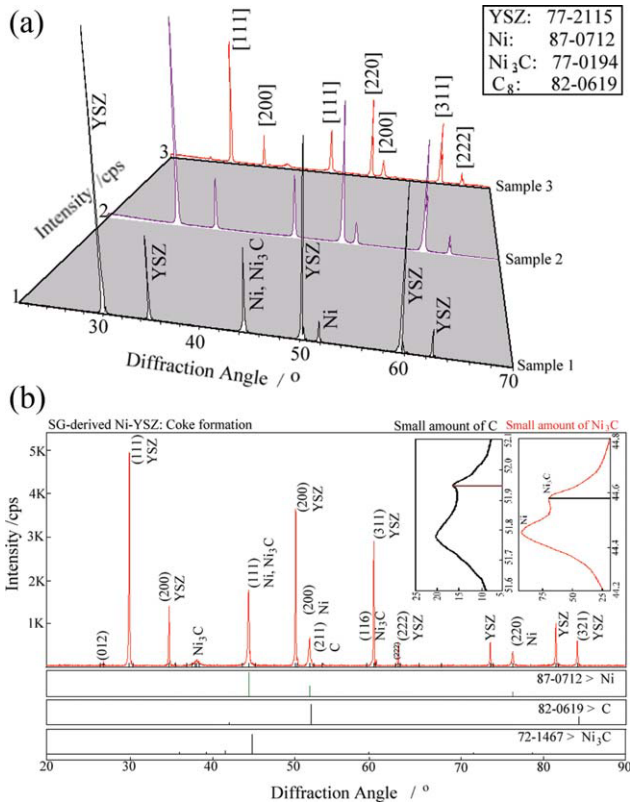

Figure 6. (a) XRD analysis of Ni-YSZ anode: three specimens finely overlap with each other; (b) XRD analysis of Ni-YSZ with preformed coke on the surface: C and Ni_3C are shown as the inserts.

[Color figure can be viewed in the online issue, which is available at www.interscience.wiley.com.]

Table 3. The Phase Percent of Anode Component and Carbonaceous Species

Species	Phase % (Compared with YSZ)	d-Spacing of Major Peak (nm)
Ni	33.6 [111]	0.204 [111]
Ni_3C	1.3 [104]	0.252 [104]
	0.4 [012]	0.336 [012]
C_8	0.4 [211]	0.175 [211]

formation. It can be seen that YSZ patterns are very well-aligned with the standard (PDF 77-2215 for YSZ and 87-0712 for Ni) as expected (see Figure 6a). Quantitatively, d-spacing of Ni ranged from 0.125 to 0.204 nm, with a negligible change after coke formation. It was found that the average Ni crystallite size for the [220] plane slightly increased from 22.9 to 24.5 nm after coke formed. This observation may also result from crystal growth under high operating temperatures.

The carbonaceous species which were formed on the surface of the Ni-YSZ anode were studied by EIS during first 4 h exposure to CH_4. To detect the carbonaceous species, the scan range varies from 51.5 to 52.5° and 44 to 45° for C_8 and Ni_3C with slow scanning rate of 0.05 degree/min. The CH_4 oxidation reaction and formation of C and Ni_3C are shown in Eqs. (4), (5), and (6).[34,37,38]

$$CH_4\ (g) = O^{2-} \rightarrow CO\ (g) + 2H_2\ (g) + 2e^- \quad (4)$$

$$CH_4\ (g) \rightarrow C_{gr}(s) + 2H_2\ (g) \quad (5)$$

$$2CO\ (g) + 3Ni(s) \rightarrow CO_2\ (g) + Ni_3C(s) \quad (6)$$

From the high resolution of XRD study, it was seen C and Ni_3C species, which were well-indexed with the standard PDF 82-0619 and 72-1467 (Figure 6 and inserts), respectively. It is important to indicate that the trace amount of C and Ni_3C species can be detected if high resolution XRD scanning is not applied.

In addition, there exists some peak overlap of C and Ni_3C with Ni. Therefore, slow scanning is critical to obtain high resolution data to interpret these spectra. From the major peak for carbon at $2\theta = 52.145°$, its phase composition was determined to be of 0.4 % from the [211] plane compared with the highest intensity from YSZ patterns. The d-spacing of C [211] is 0.175 nm. In addition, a trace amount of Ni_3C,

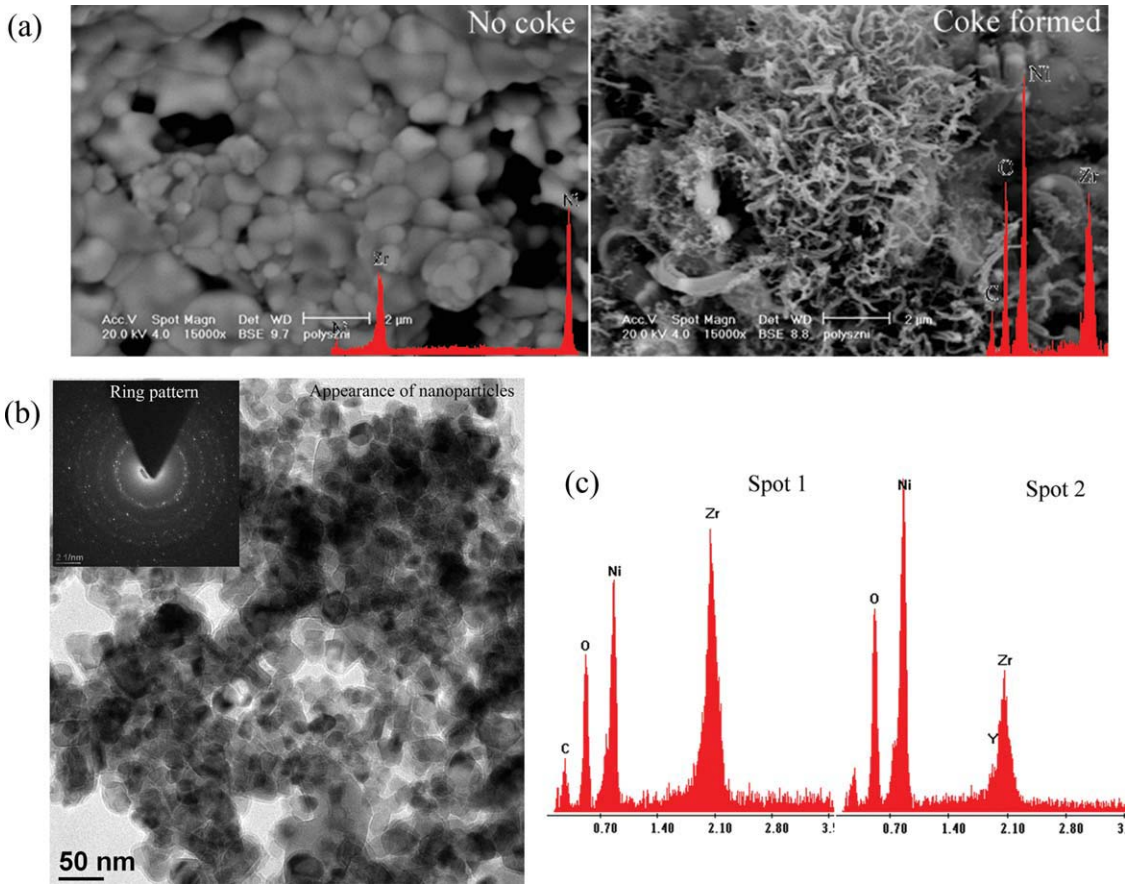

Figure 7. (a) SEM images of the outer surface of the Ni-YSZ anode: coke after exposure to 2.2 mL/min of H_2O sat. CH_4 at 800°C for 100 min; (b) TEM image of SG-derived SOFC anode nanoparticles; (c) EDS elemental composition of SG-derived Ni-YSZ/YSZ anode.

[Color figure can be viewed in the online issue, which is available at www.interscience.wiley.com.]

with a phase composition of 1.3% for the [104] plane and 0.4% for the [012] plane was seen after exposure of CH_4 to Ni-YSZ anodes. The interplanar distances of the [116], [104], and [012] planes of Ni_3C were 0.157, 0.257, and 0.336 nm, respectively. The phase percentage is shown in Table 3. Formation of Ni carbide can be explained in terms of an electronic band structure modification at the Fermi level. Carbon insertion into the Ni lattice causes a contraction of the d band width and, therefore, the lattice of cubic Ni will distort to maintain minimum lattice energy.[37]

Morphological studies by scanning electron microscope

The microstructure of the Ni-YSZ plays an important role in the performance and the stability of the electrocatalyst. Figure 7a showed that a Ni-YSZ/YSZ anode (at no coke formation) has a particle size of Ni and YSZ ranging from 0.6 to 1.5 μm. Also seen is a closely packed Ni skeleton with well-connected YSZ grains that are finely distributed over the Ni grain surfaces. The Ni-YSZ porous electrode allows gas molecules to diffuse readily. The presence of Ni-YSZ composite enhanced the triple phase boundary, resulting in the increase of electrochemically active sites.[35,38,39]

The surface morphology (Figure 7b) of a Ni-YSZ anode with coke formation generated via exposing 2.2 ml/min pure CH_4 at 800°C for 100 min was characterized. It was found that a filamentous carbonaceous product had completely coated the Ni-YSZ composite anode surface. Scanning electron microscopy (SEM) images show that a variety of carbon structures are distributed on the surface of the Ni-YSZ. Larger fibers seem to have grown from the Ni metal particles, whereas finer, spongier carbonaceous deposits tend to be distributed everywhere, in a random fashion. These growth patterns reflect the autocatalytic dehydrogenation of CH_4 on Ni to form the larger carbon fiber deposits, whereas the formation mechanism of the spongier material is less clear. The cross-sectional image of the electrolyte-supported anode allows the thickness and uniformity to be estimated. It is found that the anode is highly uniform with the thickness 20 μm as designed, which provided sufficient mechanical strength.

For the Ni-YSZ anode, covered with electrochemically deposited coke, SEM image depicted that distinguished grain boundaries were present, which favors CH_4 gas chemisorptions. However, it was also seen that the particles grow significantly when high temperature is applied. The SG-derived particles were highly monodispersed with an average size of 22.9 nm (Figure 7c), which was determined using high-resolution TEM. The ring pattern from the Ni polycrystal indicates that highly crystalline metal was obtained. However, the YSZ stays amorphous without being sintered at high temperatures, therefore, no ring pattern was obtained. The particle growth results in a dramatic decrease in the porosity and triple phase boundary, which hinders the gas diffusion and eliminates chemisorptions sites. On the other hand, this particle growth enhances the high stability of the mechanical strength; which will benefit the performance of SOFC. In other words, both electrochemical activity and mechanical stability of the SOFC must be taken into consideration. Elemental analysis (Figure 7d) performed by EDS showed that the composition Ni-YSZ anode is essentially consistent with the expected relative ratio of Ni and zirconium (Zr) to be 44:56 mass %. EDS showed that the carbon species content ranged from 7 mass % to 12 mass % from spots to spots, while the relative ratio of Ni vs. Zr slightly changed, implying lesser homogeneity, which may be another reason for the lesser reproducibility. It is reasonable to assume that the coke nucleation sites will decrease the surface temperature; therefore, the local temperature of anode surface is lowered. This is one of the reason resulting in exchange current density decreasing. On the other hand, the electrochemically active sides will be diminished due to the coke deposition, which is the major reason to cause the significant decrease of anodic kinetics.

Conclusions

From the EIS and CV data, the exchange current density for hydrogen oxidation at Ni-YSZ/YSZ anodes was found to increase exponentially from *ca.* 1.5 to 19.5 mA/cm^2 (low field CV data) by increasing the operating temperature from 600 to 800°C. After exposure to CH_4 for 4 h, the charge transfer resistance increased by more than 50% and eventually anode performance deteriorates completely due to carbonaceous species deposition on the surface of Ni. From the *ex-situ* XRD measurements, Ni and YSZ were well-indexed with the standard PDF and small amounts of C (0.4% for [211] plane) and nickel carbide (1.3% for [104] and 0.4% for [012]) formed. Based on the SEM results, it was found that a good distribution and connection between Ni and YSZ were obtained, which enabled the Ni to form a closely packed skeleton with well-connected YSZ grains that are finely distributed over the Ni grain surfaces. An elemental analysis by EDS showed the composition of the SG-derived Ni-YSZ anode was consistent with the expected relative ratio Ni:Zr = 44:56 mass %. The electrochemically generated carbonaceous species on Ni-YSZ/YSZ diminished the active sites, causing the anode deterioration.

Acknowledgments

The authors are thankful to the Alberta Energy Research Institute and Fuel Cell Energy Ltd. for financial support and provision of materials, respectively. The Course project at the University of Calgary and Texas A&M University-Kingsville (TAMUK) University Research Award (160315-00015) are duly acknowledged for the financial support. The technical support and facility access provided by the Health Center (University of Calgary) and the Department of Chemistry (University of Calgary and TAMUK), Microscopy and Imaging Center (particularly Dr. Zhiping Luo for his TEM analysis and constructive discussion) at TAMU-College Station are also acknowledged in allowing us access to state-of-the-art instrumentation and analysis software. Dr. Thomas Hays (TAMUK) is also acknowledged for copy-editing the manuscript.

Literature Cited

1. La O' GJ, In HJ, Crumlin E, Barbastathis G, Shao-Horn Y. Recent advanced in microdevices for electrochemical energy conversion and storage. *Int J Energy Res.* 2007;31:548–575.
2. Mao SS, Chen X. Selected nanotechnologies for renewable energy applications. *Int J Energy Res.* 2007;31:619–636.
3. Fu QX, Tietz F. Ceramic-based anode materials for improved redox cycling of solid oxide fuel cells. *Fuel Cells.* 2008;8:283–293.

4. Hagen A, Poulsen HF, Klemensø T, Martins RV, Honkimäki V, Buslaps T, Feidenshans R. A depth-resolved in-situ study of the reduction and oxidation of Ni-based anodes in solid oxide fuel cells. *Fuel Cells*. 2006;6:361–366.
5. Gorte J, Park S, Vohs JM, Wang C. Anodes for direct oxidation of dry hydrocarbons in a solid-oxide fuel cell. *Adv Mater*. 2000;12: 1465–1469.
6. Dicks AL. Hydrogen generation from natural gas for the fuel cell systems of tomorrow. *J Power Sources*. 1996;61:113–124.
7. Xia C, Lang Y, Meng G. Recent advances to the development of low-temperature solid oxide fuel cells. *Fuel Cells*. 2004;4:41–47.
8. Ettler M, Blaß G, Menzler NH, Characterisation of Ni-YSZ-cermets with respect to redox stability. *Fuel Cells*. 2007;7:349–355.
9. Jia J, Jiang R, Shen S, Abudula A. Effect of operation parameters on performance of tubular solid oxide fuel cell. *AIChE J*. 2008;54: 554–564.
10. Tu H, Apfel H, Stimming U. Performance of alternative oxide anodes for the electrochemical oxidation of hydrogen and methane in solid oxide fuel cells. *Fuel Cells*. 2006;6:303–306.
11. Sarantaridis D, Atkinson A. Redox cycling of Ni-based solid oxide fuel cell anodes: A review. *Fuel Cells*. 2007;7:246–258.
12. Zhu WZ, Deevi SC. A review on the status of anode materials for solid oxide fuel cells. *Mater. Sci Eng A*. 2003;362:228–239.
13. Stöver D, Buchkremer HP, Uhlenbruck S. Processing and properties of the ceramic conductive multilayer device solid oxide fuel cell (SOFC). *Ceram Int*. 2004;30:1107–1113.
14. Irvine JS, Sauvet A. Improved oxidation of hydrocarbons with new electrodes in high temperature fuel cells. *Fuel Cells*. 2001;1:205–210.
15. Y. Chang, M. Lee, W. Kao, Lin T. Preparation of a nanoscale/SOFC-grade Yttria-stabilized zirconia material: A quasi-optimization of the hydrothermal coprecipitation process. *Int J Appl Ceramic Technol*. 2008;5:557–567.
16. Kang IY, Bae JM, Yoon SH, Yoo YS. Performance improvement of diesel autothermal reformer by applying ultrasonic injector for effective fuel delivery. *J Power Sources*. 2007;172:845–852.
17. Park S, Craciun R, Vohs JM, Gorte RJ. Direct oxidation of hydrocarbons in a solid oxide fuel cell. I. Methane oxidation. *J Electrochem. Soc*. 1999;146:3603–3605.
18. Steele BH, Kelly I, Middleton PH, Rudkin R. Oxidation of methane in solid state electrochemical reactors. *Solid State Ionics*. 1988;28:1547–1552.
19. Guillodo M, Vernoux P, Fouletier J. Electrochemical properties of Ni-YSZ cermet in solid oxide fuel cells: effect of current collecting. *Solid State Ionics*. 2000;127:99–107.
20. Gazzarrij I, Kesler O. Electrochemical AC impedance model of a solid oxide fuel cell and its application to diagnosis of multiple degradation modes. *J Power Sources*. 2007;167:100–110.
21. Wang JB, Jang J, Huang T. Study of Ni-samaria-doped ceria anode for direct oxidation of methane in solid oxide fuel cells. *J Power Sources*. 2003;122:122–131.
22. Murray EP, Tsai T, Barnett SA. A direct-methane fuel cell with a ceria-based anode. *Nature*. 1999;400:649.
23. McIntosh S, Gorte RJ. Direct hydrocarbon solid oxide fuel cells. *Chem Rev*. 2004;104:4845–4866.
24. Hu YH, Feeley JS. Thermodynamic isotope effect in partial oxidation of methane to syngas. *AIChE J*. 2003;49:3253–3259.
25. Triantafyllopoulos NC, Neophytides SG. The nature and binding strength of carbon adspecies formed during the equilibrium dissociative adsorption of CH_4 on Ni-YSZ cermet catalysts. *J Catal*. 2003;217:324–333.
26. Trimm DL. Catalysts for the control of coking during steam reforming. *Catal Today*. 1999;49:3–10.
27. Young DJ. Kinetic and morphological development of coke formation on heat-resistant alloys. *Mater Corrosion*. 1999;50:675–680.
28. Kock A, De Bokx PK, Boellaard E, Klop W, Geus JW. The formation of filamentous carbon on iron and nickel catalysts. II. Mechanism. *J Catal*. 1985;91:468–480.
29. Grgicak M, Green RG, Giorgi JB. SOFC anodes for direct oxidation of hydrogen and methane fuels containing H_2S. *J Power Sources*. 2008;179:317–328.
30. Bruce PG. *Solid State Electrochemistry*, *2nd edition*. New York: Cambridge University Press, 1997.
31. Bockris J, Reddy A. *Modern Electrochemistry*, *2nd edition*. New York: Springer, 1998.
32. Liu J, Co AC, Paulson S, Birss VI. Oxygen reduction at sol-gel derived $La_{0.8}Sr_{0.2}Co_{0.8}Fe_{0.2}O_3$ cathodes. *Solid State Ionics*. 2006;177:377–381.
33. Kumar S, Chakarvarti SK, SEM morphology and XRD characterization of Ni microstructure arrays synthesized by DC electrodeposition in porous polycarbonate templates. *J Mater Sci*. 2004;39:3249–3251.
34. Li ZQ, Lu CJ, Xia ZP, Zhou Y, Luo Z. X-ray diffraction patterns of graphite and turbostratic carbon. *Carbon*. 2007;45:86–1695.
35. Yokokawa H, Tu H, Iwanschitz B, Mai A. Fundamental mechanisms limiting solid oxide fuel cell durability. *J Power Sources*. 2008;182: 400–412.
36. McIntosh S, Gorte RJ. *Chem. Rev*. 2004;104:4845.
37. Hooker P, Jit Tan B, Klabunde KJ, Suib S. Preparation of nickel carbide ultrafine particles by metal vapor methods. *Chem Mater*. 1991;3:947–952.
38. Pecharsky VK, Zavalij PY. *Fundamentals of Powder Diffraction and Structural Characterization of Materials*. New York: Kluwer Academic Publication, 2009.
39. McEvoy AJ. Activation processes, electrocatalysis and operating protocols enhance SOFC performance. *Solid State Ionics*. 2000;135:331–336.

Manuscript received Jun 11, 2009, and revision received Aug. 23, 2009.